Global anisotropic 3D FWI

Henry A. Debens, Mike Warner, Adrian Umpleby and Nuno V. da Silva, Imperial College London*

SUMMARY

Seismic anisotropy influences both the kinematics and dynamics of seismic waveforms. If anisotropy is not adequately taken into account during full-waveform seismic inversion (FWI), then inadequacies in the anisotropy model are likely to manifest as significant error in the recovered P-wave velocity model. Conventionally, anisotropic FWI uses either a fixed anisotropy model derived from tomography or such, or it uses a local inversion scheme to recover the anisotropy as part of the FWI; both of these methods can be problematic. In this paper, we show that global rather than local FWI can be used to recover the long-wavelength anisotropy model, and that this can then be followed by more-conventional local FWI to recover the detailed model. We demonstrate this approach on a full 3D field dataset, and show that it avoids problems associated to cross-talk that can bedevil local inversion schemes. Although our method provides a global inversion of anisotropy, it is nonetheless affordable and practical for 3D field data.

INTRODUCTION

In a commercial context, FWI has been used principally to recover P-wave seismic velocity, although any parameter that has an influence upon the observed seismic wavefield can in principle be estimated by FWI. For most 3D field datasets, it is necessary to include the kinematic effects of P-wave anisotropy in order to get the full benefit of FWI and to depth migrate the reflection data accurately. This anisotropy model is typically generated using reflection travel-time tomography, but it is of course possible to invert for both P-wave velocity and anisotropy during FWI, and this approach is becoming more common (da Silva et al., 2014).

Conventional FWI proceeds using a purely local inversion scheme, which can be problematic if the starting velocity and anisotropy models are not already accurate. In this paper, we explore an alternative strategy in which we combine local and global inversion methods to recover a global long-wavelength model of anisotropy together with a local high-resolution model of velocity. Hybrid inversion is feasible (Ji and Singh, 2005), even for large 3D datasets, because the required anisotropy model is much smoother than the velocity model, and so can be represented by rather few independent parameters.

THEORY

Figure 1a illustrates schematically some of the difficulties of using local inversion to recover anisotropy. In general, there is a strong trade-off between velocity and anisotropy such that the data-misfit surface tends to form narrow troughs that are oblique to both the velocity and anisotropy axes. Points A, B & C in Figure 1a represent three possible starting models; the contours show the misfit surface. For model A, the best strategy is to invert for velocity while holding the anisotropy constant; for model B, it is best to invert for anisotropy while holding velocity constant; and for model C, it is best to invert for both parameters simultaneously. Applying the wrong strategy will often lead to a worse fit to the true model.

Figure 1b shows an alternative approach. Here the inversion begins from just one velocity model represented by the horizontal line. Several anisotropy models are then chosen randomly, within some bounds, as represented by the points. Local inversion for velocity is then applied to each model as represented by the arrows. The final data misfit for each inverted model is then examined, and a new velocity model, and multi-

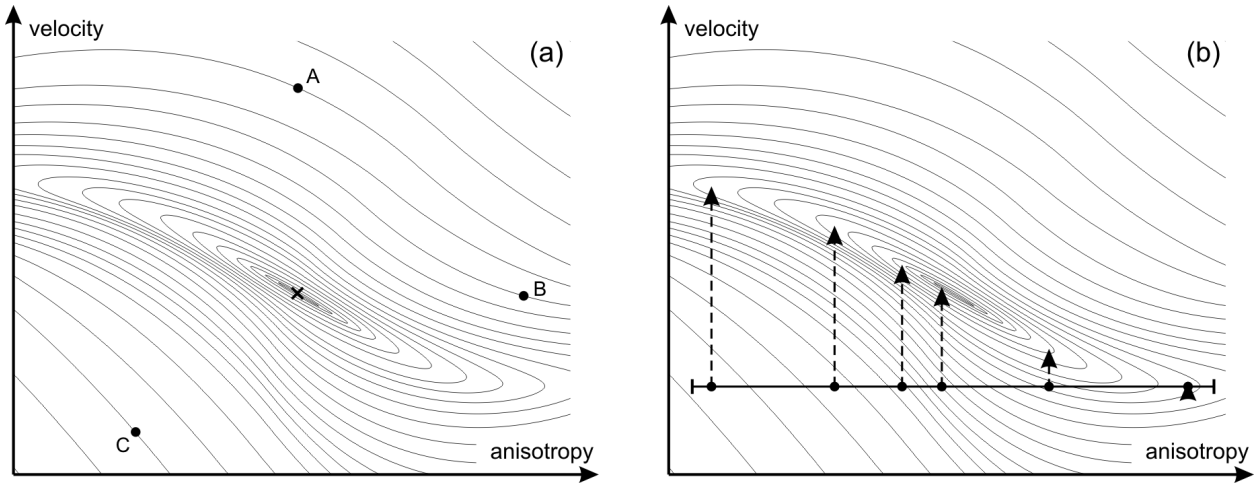

Figure 1: (a) Local inversion for three start models; (b) Global inversion for one velocity model.

DOI http://dx.doi.org/10.1190/segam2015-5921944.1

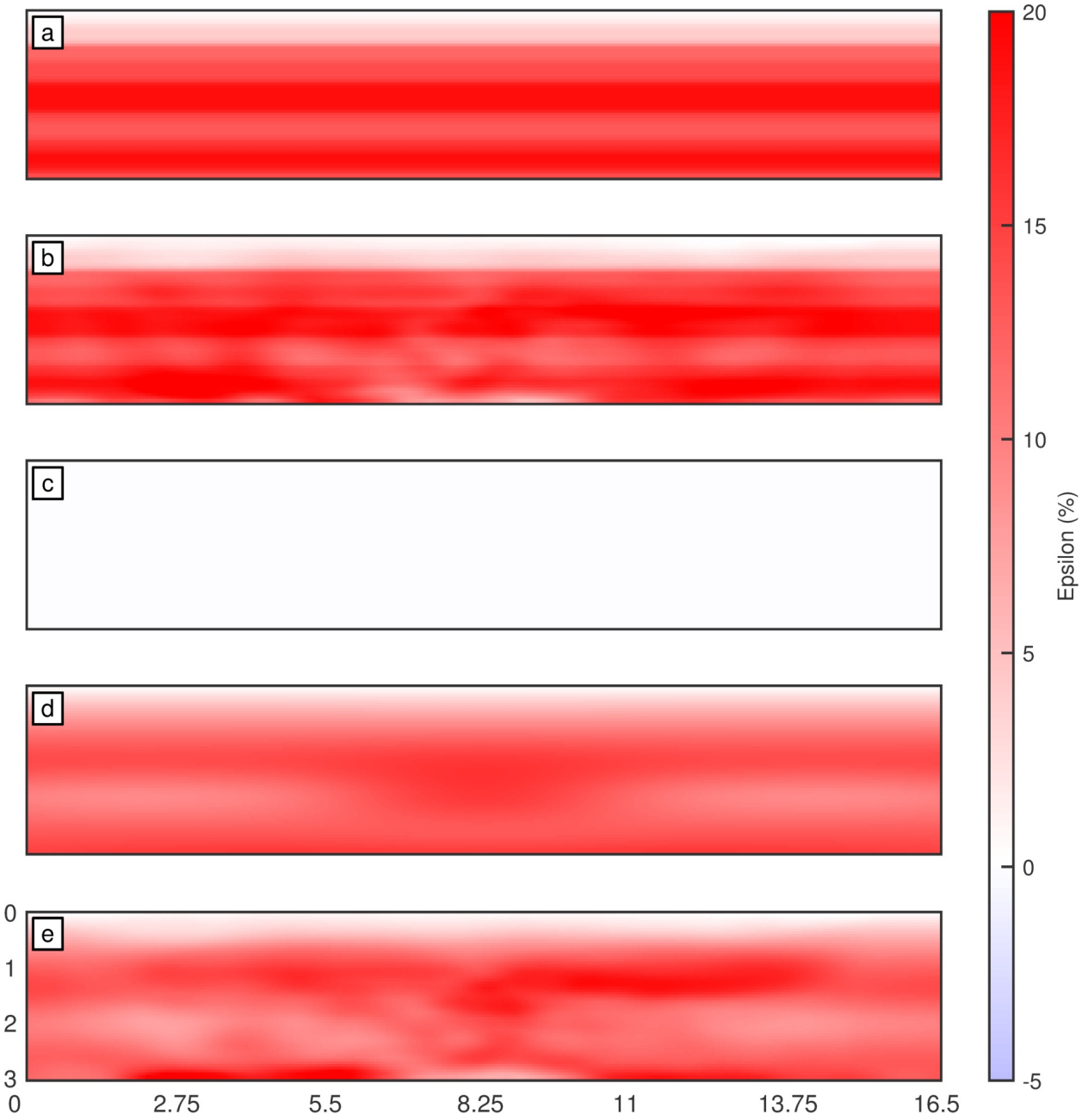

Figure 2: Vertical inline slices at 6.75 km crossline, showing the results of several multi-parameter inversions of surface seismic field data. (a) Epsilon model derived from reflection tomography; (b) model (a) after local FWI update; (c) *a priori* epsilon model for global inversion; (d) global epsilon model; (e) model (d) after local FWI update. Axes are in km.

ple new anisotropy models, are chosen statistically on the basis of these fits. In Figure 1b, these new models will tend to be chosen close to the end points of the central two models since these now have the smallest misfit. We have used quantum particle swarm optimisation (QPSO) (Sun et al., 2004) to update the anisotropy models. For a practical scheme, we found that it is only necessary to use six local iterations per global iteration, with each only using a small subset of randomised sources, to use about ten global iterations in total, and to use a population that is of a similar size to the number of anisotropy parameters required. Even in large 3D models, the latter is seldom more then a few tens of parameters for the long-wavelength anisotropy model.

Presently, we show that models produced by this approach are able to provide adequate long-wavelength information for subsequent conventional simultaneous multi-parameter FWI (Operto et al., 2013). In order to increase the impact of the diag-

DOI http://dx.doi.org/10.1190/segam2015-5921944.1

onal of the Hessian during this subsequent local inversion, we utilise a novel parameterisation, inverting for the parameters:

$$V_h + V_v$$
$$V_h - V_v \quad (1)$$

where V_h and V_v are horizontal and vertical P-wave velocities, and are related to one another by Thomsen's (1986) epsilon parameter. This parameterisation serves to rotate the axes of the misfit surface through approximately 45°, so that it becomes more closely aligned with the orientation of the data-misfit surface shown in Figure 1. This in turn allows more-effective scaling of the problem by a purely diagonal Hessian.

EXAMPLE

We demonstrate this hybrid local-global inversion scheme using a field dataset from a typical shallow-water survey in the North Sea. The survey was acquired using a high-density, full-azimuth, 3D, 4C, ocean-bottom-cable (OBC) array, with flip-flop airgun shooting taking place orthogonally to these cables. A gas condensate reservoir exists within an anticlinal fractured chalk formation, a proportion of which sits below a gas cloud in the overlying interbedded shales and sands. This gas generates a seismic-obscured zone beneath.

In this sub-horizontally-layered section, we assume vertical transverse isotropy (VTI), but our approach can deal with a tilted axis of symmetry if required. An anisotropy model for epsilon for this dataset is shown in Figure 2a. This model is based upon reflection tomography combined with well ties to a single well located near to the centre of the survey. The anisotropy model is correlated structurally with its complimentary P-wave velocity model, making cross-talk between parameters an obvious concern. In this example, due to its insensitivity in surface seismic data (Alkhalifah and Tsvankin, 1995), we do not invert for Thomsen's (1986) delta parameter, keeping it fixed throughout the inversion. In a more rigorous approach, we should recalibrate the well ties, adjusting delta as the inversion proceeds, but we have not attempted that here. Our values for delta are around half those of epsilon, so that the system is not elliptical.

During the global inversion, 12 randomly located sources (out of 1,439), were used per iteration, together with about 10,000 receivers. The source wavelet was estimated from the direct arrival and then deghosted, as an explicit free surface was used during modelling. The 3D volume covered over 200 km^2, was sampled spatially every 50 m on a regular grid, and the data were sampled at 4 ms. The anisotropic time-domain FWI algorithm used was essentially that of Warner et al. (2013), albeit modified for the rotated anisotropic parameterisation described above. Following global inversion, local inversion was employed using a multi-scale approach from 2.6 to 6.5 Hz, totalling 126 iterations where each used a subset of only 40 sources. The global inversion used a much-reduced bandwidth, incorporating no energy above 3 Hz. No *a priori* information was assumed for epsilon (Figure 2c), whilst a start model with minimal high-wavenumber information was provided for P-wave velocity by reflection tomography.

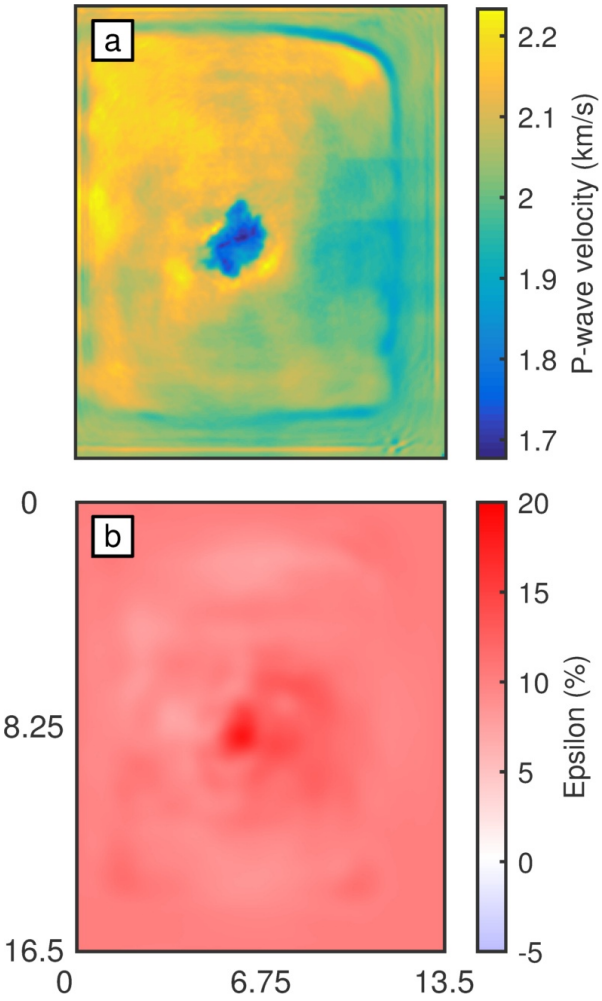

Figure 3: Horizontal slices at a depth of 2 km through: (b) the global epsilon model after local FWI update (Figure 2e), and (a) its associated P-wave velocity model. Note the presence of some inversion artefacts near the margins of the velocity model where the data fold drops off. Axes are in km.

RESULTS

The epsilon results of three multi-parameter inversions can be seen in Figure 2, together with the tomography-derived and global *a priori* models. As can be seen in Figure 2b, conventional simultaneous local FWI has had little impact on its start model, Figure 2a. It lowers epsilon in the fourth layer, between the two high-amplitude layers, and lowers epsilon towards the centre of the deepest layer. Towards the extremes of the model there is little update because of the absence of long-offset data coverage. It can be seen, especially in Figure 4, that there is high-wavenumber content in the model, which appears to be cross-talk leaking from the P-wave velocity updates.

Figure 2d shows the resultant epsilon model from the global approach. This does not begin from an individual starting model, and is constrained only by the data and by bounds on epsilon. The recovered model is qualitatively similar to the lo-

DOI http://dx.doi.org/10.1190/segam2015-5921944.1

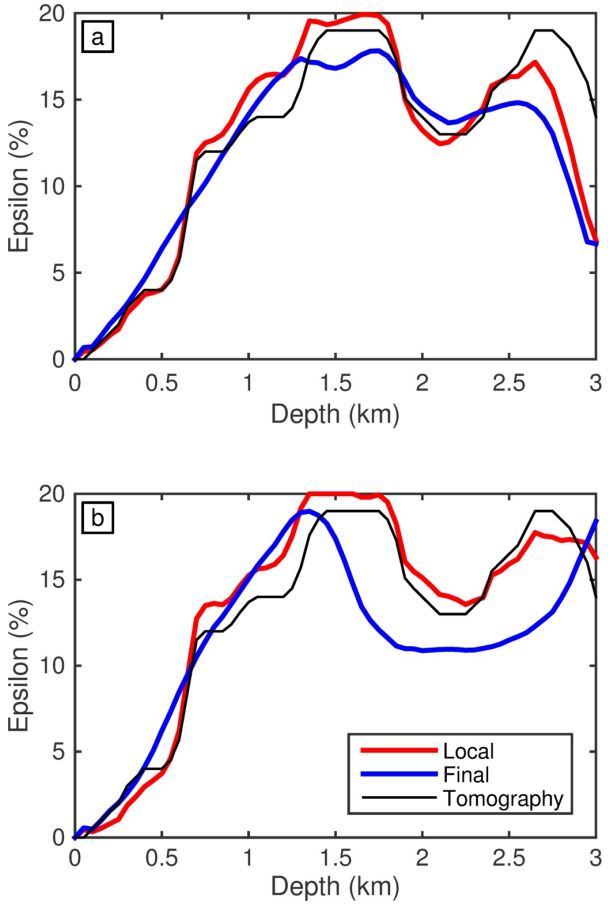

Figure 4: Model trace comparisons for epsilon at: (a) a position within, and (b) outside, the seismic obscured area. Thin black lines indicate the model derived from reflection tomography, thick red lines indicate the local FWI result, and thick blue lines indicate the result from the global approach followed by a local FWI update. Note how within the region of the gas cloud, where the well data were collected, all three models agree, whereas outside this region there is some disparity.

ng-wavelength structure in the tomography-derived model, but a key difference is the raised epsilon values in the region of the gas cloud at the centre of the model (Figure 3). We attribute the presence of anisotropy in this dataset as likely due to both aligned anisotropic minerals and fine layering between dissimilar media. The gas will be contained within the more-permeable sand-rich layers that are in turn sandwiched between gas-poor shale-rich layers. The presence of gas acts to lower P-wave velocity while leaving S-wave velocity largely unaffected. Consequently, the V_P/V_S contrast between layers is enhanced by the gas' presence, and this in turn increases the magnitude of the anisotropy in the gas-invaded region; as is seen in the global inversion.

We followed global inversion by conventional multi-parameter local FWI; the result of this can be seen in Figure 2e. Local FWI has served to push the shallow regions closer to Figure 2a, but it does this without introducing spurious cross-talk or imposing an *a priori* structure upon the epsilon model.

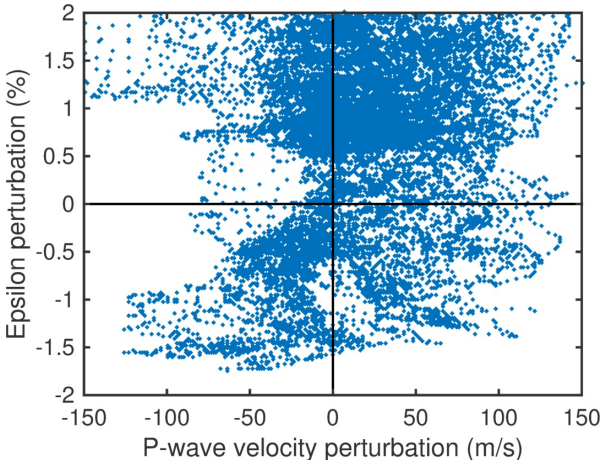

Figure 5: Crossplot of P-wave velocity and epsilon updates for the model parameters of a vertical inline slice at 11.25 km crossline in the final hybrid result. The perturbation consists of the difference between the start and final models, where the tomographic velocity model and an average of the initial epsilon model population were used as start models.

DISCUSSION AND CONCLUSION

We have presented a hybrid inversion scheme, for surface seismic data, that combines global inversion for anisotropy with local inversion for P-wave velocity. This technique extracts the long-wavelength behaviour of the anisotropy during global inversion, and then subsequently improves the velocity model at high resolution using conventional local FWI. Our methodology has been demonstrated using a typical shallow-water North Sea 3D field dataset. The approach appears to suppress cross-talk between the two inverted parameters, thus producing results of increased fidelity. This decoupling is expressed in Figure 5, where it can be seen that there is largely no correlation between velocity and epsilon updates. Because the global inversion uses low frequencies exclusively, along with roughly six local iterations per global iteration (employing heavily-decimated subsets of sources), use of this hybrid inversion scheme does not add significantly to the total cost of undertaking anisotropic FWI.

It is also possible to invert for anisotropy tilt angle using this approach, and specifically to invert for the degree to which the anisotropy is aligned with the vertical, with the stratigraphy, or with a local stress model. This approach to inverting for tilt angle requires only sparse parameterisation. It is difficult to recover tilt angles using purely local FWI, but it is inexpensive and straightforward to achieve this with the hybrid optimisation scheme outlined here.

ACKNOWLEDGEMENTS

The authors are grateful to the sponsors of the FULLWAVE Game Changer research consortium for supporting this work and releasing the field dataset.

DOI http://dx.doi.org/10.1190/segam2015-5921944.1

EDITED REFERENCES

Note: This reference list is a copyedited version of the reference list submitted by the author. Reference lists for the 2015 SEG Technical Program Expanded Abstracts have been copyedited so that references provided with the online metadata for each paper will achieve a high degree of linking to cited sources that appear on the Web.

REFERENCES

Alkhalifah, T., and I. Tsvankin, 1995, Velocity analysis for transversely isotropic media: Geophysics, **60**, 1550–1566. http://dx.doi.org/10.1190/1.1443888.

da Silva, N. V., A. Ratcliffe, G. Conroy, V. Vinje, and G. Body, 2014, A new parameterization for anisotropy update in full-waveform inversion: 84th Annual International Meeting, SEG, Expanded Abstracts, 1050–1055.

Ji, Y., and S. C. Singh, 2005, Anisotropy from full-waveform inversion of multicomponent seismic data using a hybrid optimization method: Geophysical Prospecting, **53**, no. 3, 435–445. http://dx.doi.org/10.1111/j.1365-2478.2005.00476.x.

Operto, S., Y. Gholami, V. Prieux, A. Ribodetti, R. Brossier, L. Metivier, and J. Virieux, 2013, A guided tour of multiparameter full-waveform inversion with multicomponent data: From theory to practice: The Leading Edge, **32**, 1040–1054. http://dx.doi.org/10.1190/tle32091040.1.

Sun, J., B. Feng, and W. Xu, 2004, Particle swarm optimization with particles having quantum behavior: Congress on Evolutionary Computation, 325–331.

Thomsen, L., 1986, Weak elastic anisotropy: Geophysics, **51**, 1954–1966. http://dx.doi.org/10.1190/1.1442051.

Warner, M., A. Ratcliffe, T. Nangoo, J. Morgan, A. Umpleby, N. Shah, V. Vinje, I. Štekl, L. Guasch, C. Win, G. Conroy, and A. Bertrand, 2013, Anisotropic 3D full-waveform inversion: Geophysics, **78**, no. 2, R59–R80. http://dx.doi.org/10.1190/geo2012-0338.1.